A Theoretical and Experimental Approach to Hot Tear Prediction in Steels

Robert B. Tuttle
Western Michigan University, Kalamazoo, Michigan, USA

Demitrious D. Cortez
Western Michigan University, Kalamazoo, Michigan, USA

ABSTRACT

Steel alloy development continues to provide opportunities for foundries to enter new markets. However, traditional approaches to alloy development leave the examination of manufacturing issues for the later stages of development. Introducing casting considerations earlier in the development cycle should save money and time bringing new alloys to market. The hot tearing tendency of an alloy can be predicted during the early stages of alloy design. A hot cracking index was used to compare hot tearing tendency in both previous research and from experiments poured as part of this work. Cone castings were employed to create hot tears in three different alloys. The index predicted the same pattern as the observed hot tears. Interestingly, the freezing range also correlated with the hot tearing tendency of the steels. Therefore, it appears that the hot tearing behavior of an alloy can be predicted during the early alloy development stage.

Keywords: steel, hot tear, medium manganese steels, hot tear prediction

INTRODUCTION

The development of integrated computational materials engineering (ICME) tools has led to a dramatic change in alloy development. These tools enable the metallurgist to design an alloy first from principles before conducting any experimental heats and processing. These tools also allow the metallurgist to understand how the steel will respond to processing without extensive experimentation. Calculation of phase diagrams (CALPHAD) methodology and phase field tools are currently able to predict microstructure formation and processing temperatures.[1] Defect prediction remains difficult in many cases. One particular defect that should be assessed prior to final composition selection of an experimental alloy is the tendency for hot tearing. Hot tears form when the stress in the metal exceeds its strength while it is semi-solid.[2,3] In production, these increase cost due to the need for repair welding or scrapping the casting. Hot tearing can be combated by adding more generous radii in the pattern, selecting a sand binder with better shakeout properties, or grain refinement.[4] Understanding the hot tear behavior prior to pouring an experiment would enable better alloy optimization.

Hot tearing has received significant examination in both foundry and mill environments across alloy systems.[5–12] During solidification, dendrites form within the liquid metal as freezing occurs. These dendrites continue to grow as the casting solidifies. The density of solid steel, and most metals, is higher than the liquid and causes mass to move from the liquid to the solid which develops a strain buildup.[2,3,5] Additionally, the temperature gradient within the solidification zone and casting increases the strain. Hot tearing occurs when the strain exceeds the strength of the mushy zone. In the early stages of solidification, the liquid can flow between the dendrites and “heal” the hot tear. At some point, the liquid can no longer flow due to restriction by the dendrite network.[3,13] It has been reported that this point appears to occur between 0.9 and 0.98 fraction solid in steels.[5,7,12,14]

HOT TEAR PREDICTION

Hot tear prediction has been a hot subject of research since the early 1950s.[5,10,12–15] Clyne proposed one of the first successful criterion called hot cracking susceptibility (HCS) which focused on the solidification time when the dendrite network was most susceptible to hot tearing.[14] Feurer later modified this criterion to incorporate the volumetric flow rate of the liquid into the dendrite network.[16] Rappaz, Drezet, and Gremaud (RDG) incorporated the feeding and tensile deformation of the dendrite network in their criterion, the popular RDG criterion.[17] The popularity of the RDG model stems from its ability to predict hot tearing and can be applied to product simulation. The RDG criterion cannot be used to determine the relative hot tearing susceptibility of an alloy. Kou developed a hot tearing prediction based on examining only feeding along the grain boundary.[13] The Kou model assumes that the dendrite network can be modeled as a set of hexagonal columnar grains. This leads to the following relationship between the local strain and

the growth and feeding of the dendrite network (Equation 1).

$$\frac{d\varepsilon_{local}}{dT} > \sqrt{1-\beta}\frac{d\sqrt{f_s}}{dT} + \frac{1}{(dT/dt)}\left[\left(1-\sqrt{1-\beta}\sqrt{f_s}\right)v_z\right] \quad \textbf{Eqn. 1}$$

Where T is temperature, t is time, f_s is solid fraction, ε_{local} is the local strain, β is the shrinkage, and v_z is the velocity in the negative Z direction for feeding the grain boundary. Close examination of Equation 1 finds that the $\frac{d\sqrt{f_s}}{dT}$ term becomes very negative, and cracking becomes more likely near $(f_s)^{1/2} = 1$.[13] CALPHAD tools or thermal analysis measurements can be used to determine the fraction solid verses temperature curves. Rearranging Equation 1 and examining the $\frac{dT}{d\sqrt{f_s}}$ curve provides the dendrite shape and a more interesting relationship. $\frac{dT}{d\sqrt{f_s}}$ becomes larger at $(f_s)^{1/2} = 1$, and is the slope of the T vs $(f_s)^{1/2}$ curve.

Kou concluded that computing the slope of the T vs $(f_s)^{1/2}$ curve between f_s= 0.84 and f_s= 0.94 provides a relative indication of the hot tearing tendency of an alloy.[13] The dependency of the criterion only on the fraction solid curve allows it to be combined with ICME predictions during alloy development. The metallurgist can then either use this as an additional optimization parameter or use the predictions to engineer other parts of the casting process (e.g., part radii or molding sand).

HOT TEAR EXPERIMENTS

Much like hot tearing criterions, many different casting geometries have been employed to study hot tearing. Most test castings have been some form of either a T-shaped casting or a constrained rod (Fig. 1).[5] In T-shaped castings, the lengths of the tops vary. The castings are poured and the longest length casting with a hot tear is recorded. For the constrained rod castings, various length arms that end in a sphere are on a single casting. The longest rod that cracked indicates the relative hot tearing tendency in this style of casting.

A significant disadvantage to these styles of test castings is their discrete nature. Alloys with slightly different hot tearing tendencies may appear similar due to the limited number of rod lengths. Recent attempts to resolve this issue by academic researchers has focused on adding sensors to the ends of either T-shaped or cylindrical castings. These instrumented test castings provide data on the strength of the mushy zone and the strain sensitivity of the alloy by the application of an applied force. However, these are not good test castings for an industrial setting or simple verification of the relative hot tearing behavior of a new alloy during early trials.

Trikha and Bates conducted research on hot tearing in steel castings using a unique cone geometry.[18] Figure 2 depicts this geometry. The concept is that the cone shape results in a difference in contraction between the small and large diameters of the casting. A hot tear tends to form on the inside of the casting adjacent to the knife gate. The length of the hot tear is measured and then compared. The result is a measurement system that results in a continuous measurement of hot tearing, not discrete. Thus, slight differences in hot tearing tendency between alloys can be detected.

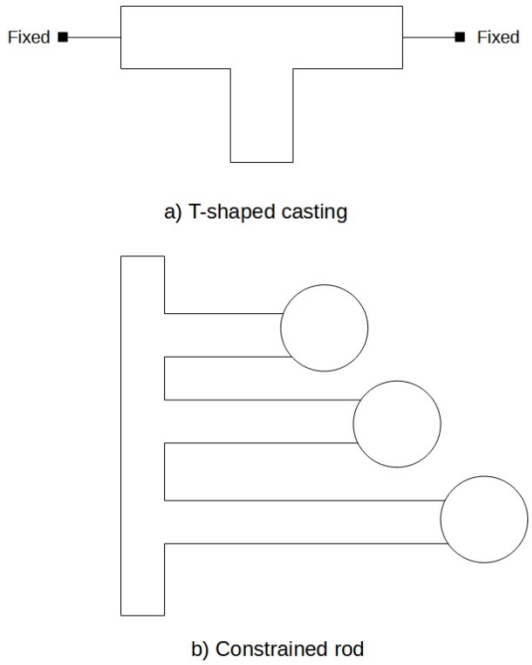

Figure 1. Typical hot tear castings.

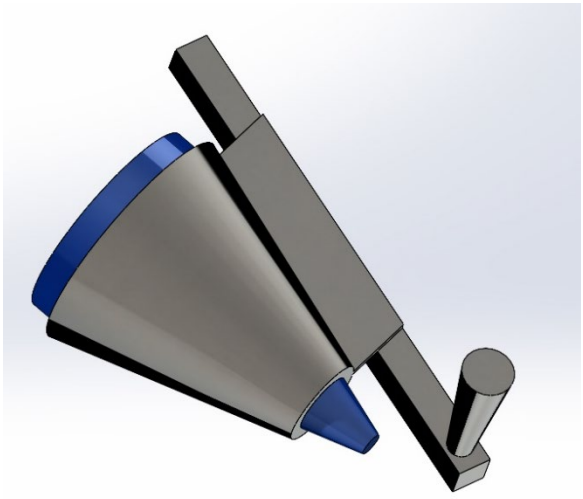

Figure 2. Hot tear cone casting with core (blue).

Trikha and Bates experimented with 1025, CF-3, and CF-8 alloys. They also examined sodium silicate and ester cured phenolic nobake binders in the cores. CF-8 and 1025 were found to have similar hot tearing tendency while CF-3 was less prone.[18] They also observed that core density and binder type also had strong effect on hot tearing.[18]

The goal of this paper was to determine the applicability of the Kou hot tear criterion in steel. First, predictions were made using data from the Trikha and Bates paper to determine if the Kou criterion predicted the observed alloy trends. Next, predictions were made for a heat of WCB steel and a medium-manganese steel which were then poured using the same cone test casting. The medium-Mn steel was selected due to recent interest in these alloys.[19–28] A heat of 1025 was also poured to determine if there were significant differences between these experiments and the Trikha and Bates paper.

EXPERIMENTAL PROCEDURE

HOT TEAR PREDICTION

For the initial predictions, the composition of each steel from the Trikha and Bates work was used to conduct Scheil calculations in ThermoCalc© using the TCFE 12 database and a fast diffusion assumption for carbon (Table 1). These results were then exported and analyzed in R (Ver 4.3.0). The R program consisted of data input and then computing the slope of the T vs $(f_s)^{1/2}$ curve for each alloy with the general linear model. This was then compared to the length data from the Trikha and Bates paper.

For predictions, the same approach was employed for WCB and a medium manganese (Med-Mn) steel. Table 2 lists the compositions.

Table 1. Compositions from Trikha and Bates in Wt. %

Alloy	C	Cr	Ni	Mn	Si	Mo	S	P
1025	0.24	0.41	0.13	0.91	0.58	0.04	0.012	0.022
CF-3	0.02	17.8	9.18	0.82	1.29	0.15	0.001	0.012
CF-8	0.06	19.7	9.14	0.86	1.28	0.20	0.006	0.024

Table 2. Target Compositions for Scheil Predictions of Experimental Alloys in Wt. %

Alloy	C	Mn	Si	Al
WCB	0.29	1.0	0.2	0.1
Med-Mn	0.20	2.5	1.7	0.1

CASTING TRIALS

To verify the WCB and Medium-Mn predictions, a set of experimental heats were poured. A slight modification to the original Trikha and Bates casting was made (Fig. 3). A swirl dirt trap was added to the end to assist with capturing slag from the ladle and any inclusions formed during initial filling. Molds and cores were made from a silica molding sand with a 55 AFS GFN and 2 wt. % ester cured phenolic nobake resin binder. Two test castings were poured per alloy.

A 3 kHz induction furnace with an alumina crucible melted the 23 kg heats of 1025, WCB, and Med-Mn steels in air. The initial charge consisted of 1010 punchings. Once molten, FeSi, electrolytic manganese, and graphite were added for final composition. The furnace was tapped at 1730C (3146F) into a preheated ladle lined with a magnesia based fiber refractory. The test castings were poured at 1610C (2930F) and allowed to cool to room temperature before shakeout. Table 3 lists the final heat compositions.

After shakeout, the castings were abrasive blasted. A small amount of grinding at the hot tear was done using a die grinder with a carbide burr to ensure the entire hot tear was exposed. The hot tear length was then recorded. Images of the hot tear were also captured.

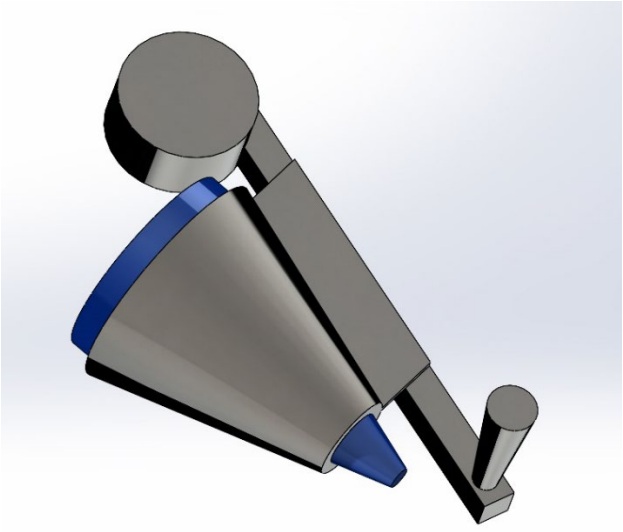

Figure 3. Modified cone casting utilized in this work.

Table 3. Heat Compositions in Wt. %

Alloy	C	Mn	Si	Al
1025	0.23	0.68	0.27	0.09
WCB	0.29	1	0.2	0.1
Med-Mn	0.25	3.38	1.74	0.03

RESULTS AND DISCUSSION

HOT TEAR PREDICTION

Analysis began with the steels from the Trikha and Bates paper. Figures 4 through 6 present the solid fraction curves from the Scheil analysis. The liquidus, solidus, and freezing range for each alloy are listed in Table 4.

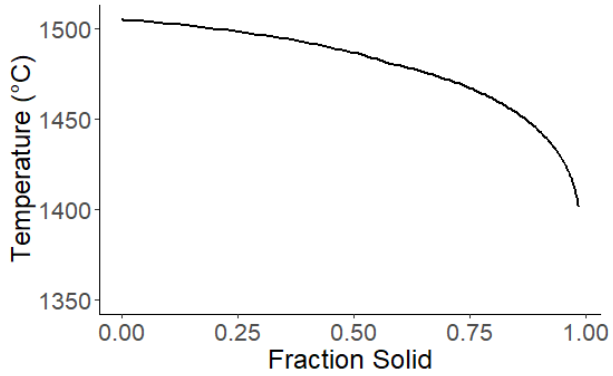

Figure 4. Solid fraction curve for 1025.

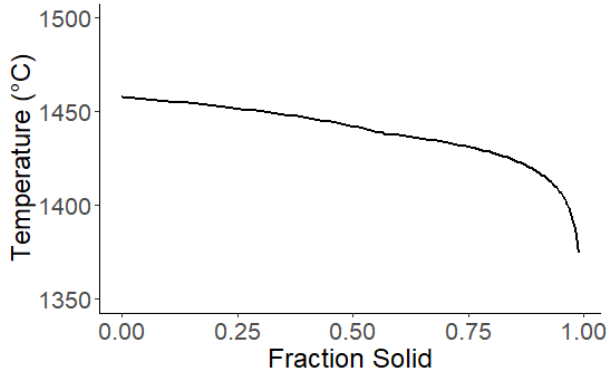

Figure 5. Solid fraction curve for CF-3.

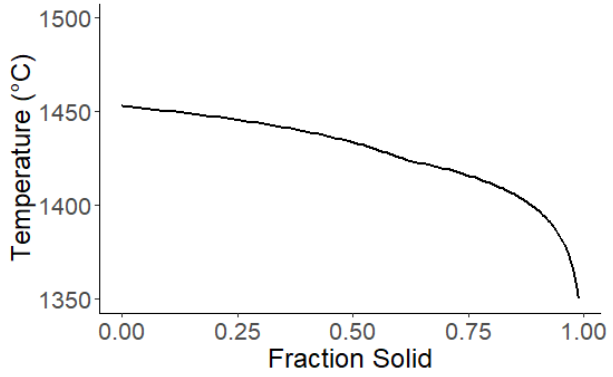

Figure 6. Solid fraction for CF-8.

Table 4. Solidification Temperatures for Alloys.

Alloy	Liquidus (°C)	Solidus (°C)	Freezing Range
1025*	1505	1401	104
CF-3	1457	1374	83
CF-8	1453	1350	104
WCB*	1508	1146	362
Med-Mn*	1487	1339	148

* Alloys poured in current work.

The hot tearing index for each alloy in the Trikha and Bates paper is shown in Figure 7 along with the average hot tear length.[18] The hot tear index changes matched the hot tear length trends observed in their work. Trikha and Bates noted the hot tear tendency of 1025 and CF-8 was similar while CF-3 had a lower tendency. This seems associated with 1025 and CF-8 having a larger freezing range which also correlates to a larger dendrite length at the same cooling rate.[2] Replotting the hot tear length and freezing range for each alloy indicates a similar trend (Fig. 8). Kou's hot cracking index makes the differences between alloys appear larger.

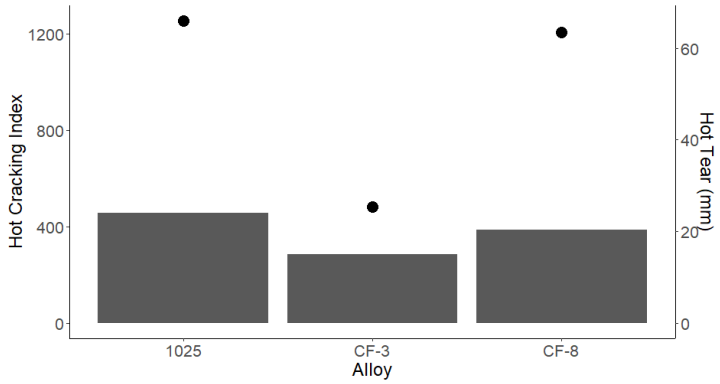

Figure 7. Hot tear index (columns) and hot tear length (dots) for Trikha and Bates data.

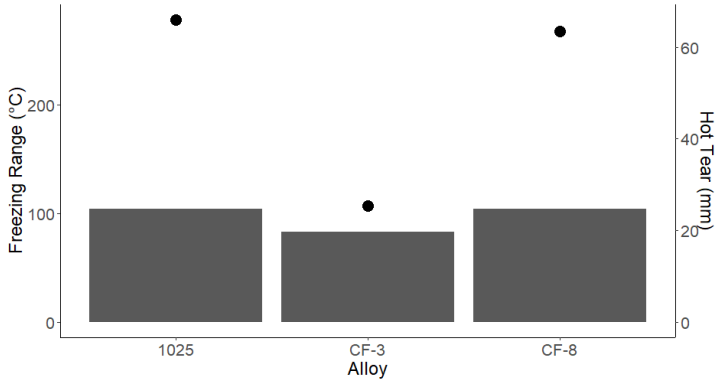

Figure 8. Freezing range (columns) and hot tear length (dots) for Trikha and Bates data.

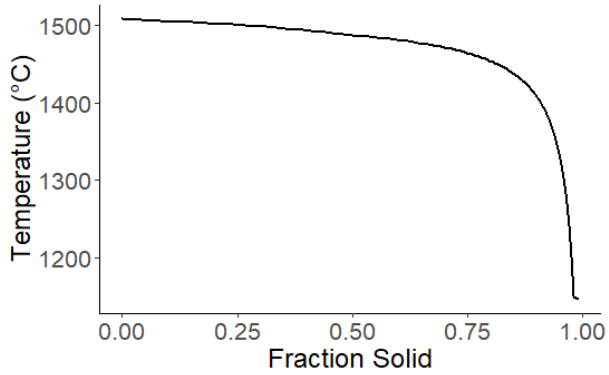

Figure 9. Solid fraction curve for WCB.

The solid fraction curves for WCB and the Med-Mn steel were computed (Figs. 9 and 10). WCB has the longest freezing range of the alloys investigated (Table 4). The Med-Mn steel appears to have a larger freezing range than the steels in the Trikha and Bates experiments. The hot cracking index was 1636 for WCB and 638 for the Med-Mn steel. This would indicate both should have a higher hot tearing tendency than the steels from the Trikha and Bates work.

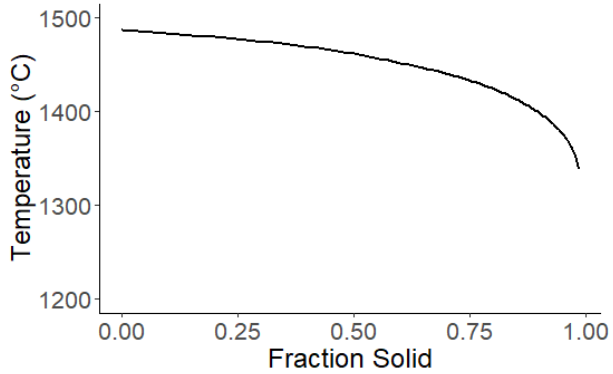

Figure 10. Solid fraction curve for Med-Mn alloy.

CASTING TRIALS

Casting trials were conducted for the 1025, WCB, and Med-Mn steels. Only one hot tear was observed in the 1025 castings and is presented in Figure 11. Figure 12 provides a representative image of a hot tear in a WCB casting while Figure 13 depicts a typical hot tear in the Med-Mn steel. Figure 14 presents the average hot tear length and index prediction for each alloy.

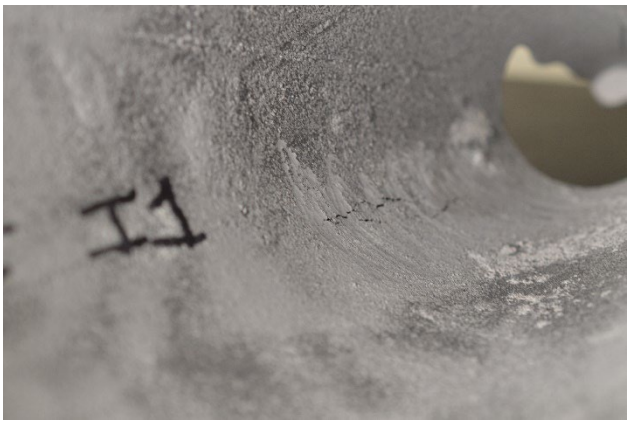

Figure 11. Hot tear from first casting of 1025.

Figure 12. Typical hot tear in WCB casting.

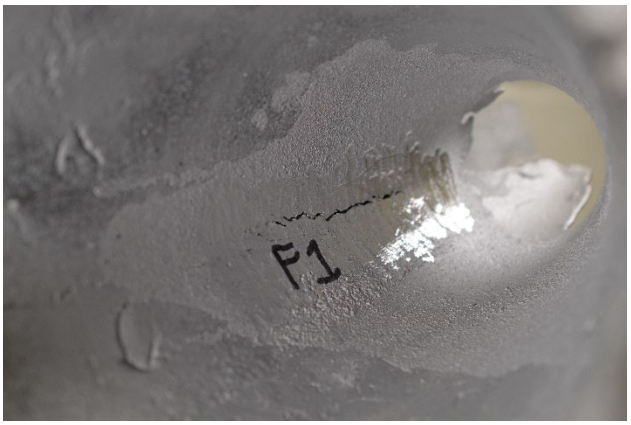

Figure 13. Typical hot tear in Med-Mn steel.

The trend found in Figure 14 mirrors the trends in the index and presented in the Trikha and Bates data. The higher the index the longer the hot tear observed. This trend also matches with the change in freezing range (Fig. 15). It should be noted that the observed hot tear average in 1025 was more than half of that found in the original Trikah and Bates paper.[18] There are several possible causes, such as different aggregate sands, binder differences, and core density.

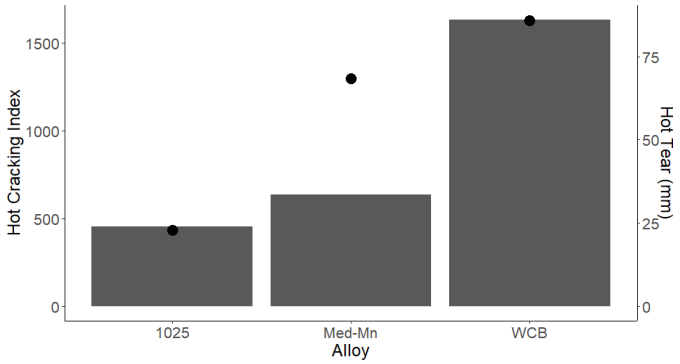

Figure 14. Hot tear index (columns) and hot tear length (dots).

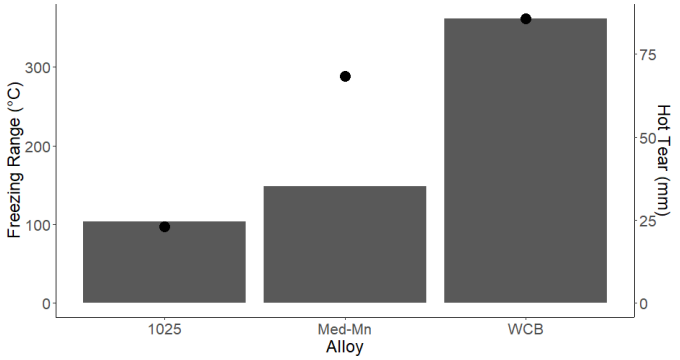

Figure 15. Freezing range (columns) and hot tear length (dots).

Another interesting observation made during the experiment was that the first test casting in each heat tended to have a longer hot tear than the second casting. Thus, the longest hot tears for the 1025, WCB, and Med-Mn steel were 46, 108, and 50.8 mm respectively. This likely occurred due to the slightly higher pouring temperature of the first casting. A higher pouring temperature should result in a larger residual stress developing during solidification, thus also producing a longer hot tear. It is additionally interesting to note that the maximum hot tear lengths for 1025 and Med-Mn appear closer, mirroring the hot cracking index and freezing range differences.

The fact that the hot cracking index and freezing range provide similar results regarding the hot tearing tendency in both the current work and Trikah and Bates experiments leads to the question of why not simply use the freezing range. As is generally known, it has been long standing practice to subjectively evaluate alloys for hot tearing based on the freezing range of the alloy. Kou's analysis provides some basis for this in regards to the temperature distribution along the dendrite where a larger freezing range simply results in a longer dendrite that is harder for the interdendritic liquid to feed.[13] However, Kou's criterion would be capable of determining hot tearing tendencies between alloys with similar freezing ranges. Re-examining Table 4 indicates that 1025 and CF-8 have a similar freezing range but have different hot cracking indices due to the higher slope of the fraction solid curve towards the end of solidification. While not statistically significant according to Trikha and Bates, there is a slight difference in the observed hot tear length between these two alloys with CF-8 having a lower tendency and index.[18] Figure 16 depicts the relationship between the hot cracking index and freezing range for all alloys discussed in this paper. There is a strong correlation between the two.

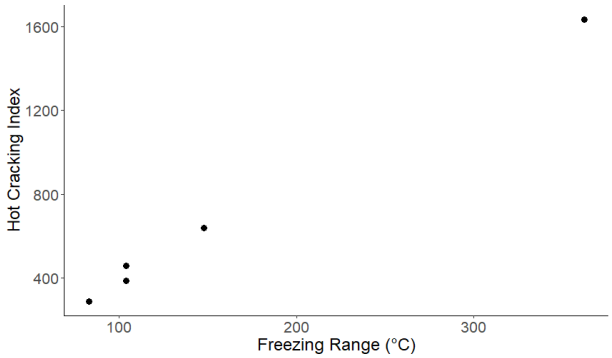

Figure 16. Index vs. freezing range for all alloys.

For there to be a significant difference between the trend indicated by changes in the freezing range and the hot cracking index, the slope of the solid fraction curve towards the end of solidification would need to be significantly different for the same temperature range. Figure 17 depicts such a theoretical possibility. The alloy with the higher slope towards the end of solidification would have a higher hot tearing tendency than the one with the lower slope. Kou's index would detect this, but the traditional rule of using the freezing range would not. Using only the freezing range as a criterion, both alloys would appear to have the same hot tearing tendency. However, the author is not aware of such a situation existing. Thus, it would seem simply using the freezing range provides a good indicator during the early stages of alloy design. Kou's work presents the theoretical background on why this occurs.

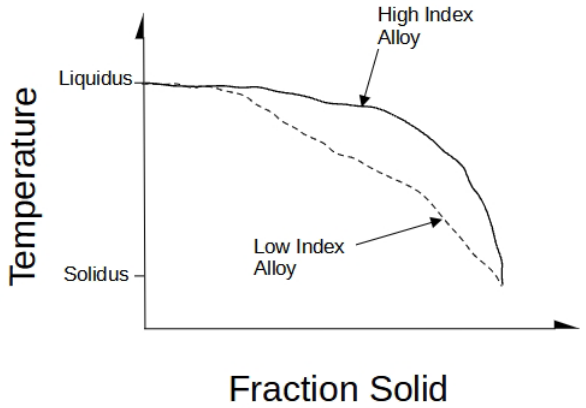

Figure 17. Situation where alloys have same freezing range but different hot cracking indices.

CONCLUSIONS

WCB tended to have the largest hot tears followed by the Med-Mn steel and then 1025. The hot tear length for 1025 in the current work was much lower than in research by previous authors. Computation of the hot cracking index predicted a similar trend as observed in the experimental data as did the freezing range.

It appears that the freezing range provided as good a prediction of hot tearing tendency as the hot cracking index. Plotting the two together for all data sets resulted in an almost one-to-one correlation. The author postulates that it is possible for two alloys to have the same freezing range, but a different slope at the end of solidification. This difference in slope would result in a different hot cracking index. However, the necessary fraction solid curve shape did not match any known alloy. Thus, while theoretically there might be a difference, it appears simply using the freezing range during alloy development provides a reasonable estimate of hot tearing behavior.

ACKNOWLEDGMENTS

The authors would like to thank Mujeeb Shiak and Jacob Paquette for their assistance in pouring this casting. Further they appreciate Jennie Tuttle's editorial assistance. Finally, the authors would like to thank the LSAMP program for providing funding to support this work.

REFERENCES

1. Lukas, H.L., Fries, S.G. & Sundman, B., "Computational Thermodynamics: The CALPHAD Method," Cambridge University Press, Cambridge, New York (2007).
2. Stefanescu, D., "Science and Engineering of Casting Solidification," Springer, New York, NY (2015).
3. Dantzig, J. & Rappaz, M., "Solidification," EPFL Press, Lausanne; London (2009).
4. Tuttle, R.B., "Foundry Engineering: The Metallurgy and Design of Castings," Independently Published (2020).
5. Lu, Y., Bartlett, L.N. & O'Malley, R.J., "A Review on Hot Tearing of Steels," *International Journal of Metalcasting*, vol. 16 (1), pp. 45–61 (2022).
6. Monroe, C. & Beckermann, C., "Development of a Hot Tear Indicator for Use in Casting Simulation," *Proceedings of the 58th SFSA Technical and Operating Conference*, pp. 1–13 (2004).
7. Monroe, C. & Beckermann, C., "Development of a Hot Tear Indicator for Steel Castings," *Materials Science and Engineering: A*, vol. 413–414, pp. 30–36 (2005).
8. Neff, D., "Aluminum Casting Technology," American Foundry Society, Schaumburg, IL, (2017).
9. Coniglio, N. & Cross, C.E., "Mechanisms for Solidification Crack Initiation and Growth in Aluminum Welding," *Metallurgical and Materials Transactions A*, vol. 40 (11), pp. 2718–2728 (2009).
10. Davidson, C., Viano, D., Lu, L. & St. John, D., "Observation of Crack Initiation during Hot Tearing," *International Journal of Cast Metals Research*, vol. 19 (1), pp. 59–65 (2006).
11. Eskin, D. G., Suyitno & Katgerman, L., "Mechanical properties in the semi-solid state and hot tearing of aluminium alloys," *Progress in Materials Science*, vol. 49 (5), pp. 629–711 (2004).
12. Yan, F., Yan, J. & Linder, D., "Understanding Hot Cracking of Steels during Rapid Solidification: An ICME Approach," *The 1st International Electronic Conference on Metallurgy and Metals*, pp. 30 (2021).
13. Kou, S., "A criterion for cracking during solidification," *Acta Materialia*, vol. 88, pp. 366–374 (2015).
14. Clyne, T.W., Wolf, M. & Kurz, W., "The effect of melt composition on solidification cracking of steel, with particular reference to continuous casting," *Metallurgical Transactions B*, vol. 13 (2), pp. 259–266 (1982).
15. Schneider, M.C. & Andersen, S., "Simulated Analysis of Macrosegregation, Hot Tears and Heat Treatment in Steel Castings," *Transactions of the American Foundrymen's Society*, vol. 107, pp. 547–554 (1999).
16. Suyitno, Kool, W.H. & Katgerman, L., "Hot tearing criteria evaluation for direct-chill casting of an Al-4.5 pct Cu alloy," *Metallurgical and Materials Transactions A*, vol. 36 (6), pp. 1537–1546 (2005).
17. Rappaz, M., Drezet, J.-M. & Gremaud, M., "A new hot-tearing criterion," *Metallurgical and Materials Transactions A*, vol. 30 (2), pp. 449–455 (1999).
18. Trikha, S.K. & Bates, C.E., "Improved Method for Hot Tear Testing and Methods to Reduce Hot Tears," *Transactions of the American Foundrymen's Society*, vol. 102, pp. 173–180 (1994).

19. Cao, R., Liang, J., Li, F., Li, C. & Zhao, Z., "Intercritical Annealing Processing and a New Type of Quenching and Partitioning Processing, Actualized by Combining Intercritical Quenching and Tempering, for Medium Manganese Lightweight Steel," *Steel Research International*, vol. 91 (1), pp. 1900335 (2020).
20. Gao, P., Li, F., An, K., Zhao, Z., Chu, X. & Cui, H., "Microstructure and Deformation Mechanism of Si-strengthened Intercritically Annealed Quenching and Partitioning Steels," *Materials Characterization*, vol. 191, pp. 112145 (2022).
21. Prueger, S., Kuna, M., Wolf, S. & Krueger, Lutz., "A Material Model for TRIP-Steels and its Application to a CrMnNi Cast Alloy.," *Steel Research International*, vol. 82, pp. 1070–1079 (2011).
22. Glage, A., Weidner, A. & Biermann, H., "Cyclic Deformation Behaviour of Three Austenitic Cast CrMnNi TRIP/TWIP Steels with Various Ni Content," *Steel Research International*, vol. 82 (9), pp. 1040–1047 (2011).
23. Grajcar, A., "Segregation Behaviour of Third Generation Advanced High-Strength Mn-Al Steels," *Archives of Foundry Engineering*, vol. 12 (2) (2012).
24. Qu, H., Michal, G.M. & Heuer, A.H., "Third Generation 0.3C-4.0Mn Advanced High Strength Steels Through a Dual Stabilization Heat Treatment: Austenite Stabilization Through Paraequilibrium Carbon Partitioning," *Metallurgical and Materials Transactions A*, vol. 45 (6), pp. 2741–2749 (2014).
25. Wang, H., Kang, J., *et al.*, "Microstructure and mechanical properties of hot-rolled and heat-treated TRIP steel with direct quenching process," *Materials Science and Engineering: A*, vol. 702, pp. 350–359 (2017).
26. Mohammadi Zahrani, M., Ketabchi, M. & Ranjbarnodeh, E., "Microstructure Development and Mecanical Properties of a C-Mn-Si-Al-Cr Cold Rolled Steel Subjected to Quenching and Partitioning Treatment," *Journal of Materials Research and Technology*, vol. 22, pp. 2806–2818 (2023).
27. Del Molino, E., Arribas Telleria, M., *et al.*, "Influence of Ni and Process Parameters in Medium Mn Steels Heat Treated by High Partitioning Temperature Q&P Cycles," *Metallurgical and Materials Transactions A*, vol. 53 (11), pp. 3937–3955 (2022).
28. Wang, J., Qian, R., Yang, X., Zhong, Y. & Shang, C., "Effect of Segregation on the Microstructure and Properties of a Quenching and Partitioning Steel," *Materials Letters*, vol. 325, pp. 132815 (2022).